Dissolution of CO_2 and CH_4 Bubbles and Drops Rising from the Deep Ocean

Giulia Bozzano* and Mario Dente

Politecnico di Milano, Dipartimento di Chimica, Materiali e Ingegneria Chimica "Giulio Natta", Piazza Leonardo da Vinci 32 20133 Milano, Italy

1. INTRODUCTION

Hydrates of natural gases are widely distributed in marine sediments. The natural deposits of gas hydrates are estimated to hold higher reserves than all known conventional gas reservoirs.[1−3] Their proximity to the seafloor has motivated an interest toward the study of a release of methane. It could be a consequence of the increase in temperature or decrease in pressure (through changes in sea level), or by slumping of continental slopes. Incidentally methane has a greenhouse effect from 21 to 25 times higher than CO_2.[4] Hydrate decomposition has been also suggested to trigger slope failures with a consequent release of a larger amount of the greenhouse gas.[5] The study of CO_2 drops dissolution into see water has been initially stimulated by the interest toward the ocean sequestration.[6] One of the original ideas was to release liquid CO_2 at ocean depths where CO_2/seawater density inversion is reached or to replace into the clathrates methane with CO_2[7] because of the isotypical structure[8] of CO_2 and CH_4 clathrates in symilar equilibrium conditions. CO_2 ocean storage, however, has been recently[9] considered to be too dangerous regarding local environmental impacts (ocean acidification). In the mean time, carbon capture and sequestration in subsea geological formations (CCS-SSGF) for permanent isolation is still an alternative and has been regulated by the London Convention.[10]

A further disadvantage of ocean sequestration is that the CO_2 injection must be realized at deep of at least 1000 m to prevent outgassing and could therefore be a very expensive.

Liquid CO_2 release can be related to the accidental leakage from subsedimentarily stored CO_2. There have been discussions about CO_2-dominated hydrates naturally occurring from sea floor volcanic emissions. In 1988 such a site was discovered in the Okinawa Trough at a depth of 1300−1500 m and 3.8 °C. Submarine explorations in 1989 by a Japanese team[11]revealed hot (320 °C) black-smoker vents, and they observed unusual bubbles emerging nearby. The gas analysis showed the following composition: 86% CO_2, 3% H_2S, 11% (CH_4 + H_2). The CO_2-rich gas, upon venting into superficial sediments bathed in 3.8 °C water, was condensing into the liquid state and forming a hydrate shell.[12]

All these aspects emphasize the importance of the study of the release of these gases from the deep ocean. Since the seawater is usually undersaturated in both CO_2 and CH_4, they dissolve in the water column and, eventually, are released into the atmosphere. In all the situations, when CO_2 and CH_4 drops and/or bubbles are present, their behavior is dictated by hydrodynamics, deformation of the fluid particles, formation and dissociation of hydrates, and mass transfer and dissolution of the particles. All these aspects have to be taken into account in order to adequately model the dissolution process.

An important aspect of this modeling is the characterization of the particles (bubbles or drops) terminal rise velocity. This latter is a function of their size and shape during motion and of the eventual presence, under proper P/T conditions, of clathrates at the interface.[13,14] Mainly in the case of gases, the particle size depends also on the pressure variation along the path. Laboratory[15−18] and ocean[19−21] experiments have been extensively performed to assess the fate of CO_2 and CH_4 rising in the water columns. Model calculation have been also performed,[22−26] mainly based on empirical correlations.

Regarding the particle "terminal" rise velocity, Gangstö et al.[24] adopted a model[27] developed for gas−liquid systems for evaluating the rise velocity of CO_2 drops. Obviously, the match with experimental data was not completely satisfactory. Starting from the same paper[27] and adopting the same assumption for evaluating particle deformation, Bigalke et al.[28] obtained an expression for the deformation factor as a function of Weber ($We = (D_0\rho_c v_p^2)/\sigma$) and Eötvös ($Eo = (\Delta\rho g D_0^2)/\sigma$) numbers ($D_0$ = diameter of the equivalent spherical fluid particle, ρ_c density of the continuous phase, σ = interfacial tension, v_p particle velocity, $\Delta\rho$ = density difference between continuous and dispersed phase, g = gravitational acceleration).

Received: October 2, 2013
Revised: February 6, 2014
Accepted: February 7, 2014
Published: February 7, 2014

They proposed two expressions for the friction factors of particles covered and uncovered by hydrates. They obtained a model function of dimensionless numbers affecting the shape and the friction factor of the particles, having the advantage of being applicable to hydrate-coated and hydrate-free CO_2 droplets as well as hydrate-coated CH_4 bubbles. Their conclusion was that further effort should be addressed to the characterization of dissolution in presence of hydrates in order to have unique models treating CH_4 and CO_2 particles dissolution in deep sea.

In this paper, we present a new procedure for evaluating dissolution rate that is based on a general model for the prediction of particle rise velocity. It has not been specifically developed for the case of CO_2 and CH_4 particles, but takes into account the unique aspects related to the oceanic environment (i.e. the effect of salinity, of pressure, the presence of hydrates). The concepts here reported were initially adopted for gas–liquid systems[27] and, subsequently, extended to liquid–liquid systems.[29] Particle dissolution and the effect of hydrate skin on mass transfer are modeled. The comparisons with some of the experimental data reported into the literature are satisfactory.

2. DISSOLUTION MODEL

From the chemical engineering point of view, the phenomena to be described, which means drops and/or bubbles to be dissolved in a liquid medium, do not present particularly difficult aspects. In facts, many of the equipments typical of the chemical engineering unit operations involve motion and rate of exchange of drops and bubbles. However, at least two conditions are quite exceptional in the case under consideration, if compared with the typical conditions of the chemical engineering equipments. The first one is the height of the oceanic seawater column, which, as a result of the hydrostatic pressure, produces a drastic variation of the density and volume of the fluid inside the liquid or gas particles along their path. The second one is the formation, presence, and disappearance of the hydrates at the interface between the particle and surrounding, low temperature, seawater. The first of these two aspects generates a large variation of the pressure inside the particles. It only requires the use of a reasonable and well recognized equation of state in order to properly evaluate the density of the fluid (gas, liquid, or gas–liquid mixtures if vaporization inside the particles takes place of course at relatively low shallow thickness such as 400/500 m). In this work, the preferred equations of state for CO_2 and CH_4 has been the Peng–Robinson EoS,[30] while clathrate stability and existence has been evaluated by using the equation of Patel and Teja.[31] The interfacial tension of the liquid CO_2 and seawater has been evaluated by adopting the following combination of the superficial tension of CO_2 and seawater:[32]

$$\sigma_{CO_2-SW} = (\psi^{\sigma}_{SW}\sigma^{0.25}_{SW} + \psi^{\sigma}_{CO_2}\sigma^{0.25}_{CO_2})^4 \tag{1}$$

where $\psi^{\sigma}_i = (x_iV_i)/V$ (i = SW or CO_2); x_i = mole fraction of i in the surface layer; V_i = pure liquid molar volume of i; σ_i = surface tension of i; $V = \sum_i x_iV_i$.

The mole fraction of CO_2 at the interface has been calculated by adopting the modified Henry's Law,[33] and as reported in ref 34:

$$x_{CO_2} = \frac{f_{CO_2}}{H} \tag{2}$$

where x_{CO_2} is the solubility of CO_2 in water and f_{CO_2} and H are, respectively, the fugacity of liquid CO_2 and the Henry's law constant at T and p. The Henry constant is evaluated as[34]

$$H = a + pP + cP^2$$
$$a = 5.2 \times 10^4 - 392T + 0.75T^2$$
$$b = -103 + 0.708T - 1.2 \times 10^{-3}T^2$$
$$c = 2.2 \times 10^{-3} \quad (P\text{: MPa; } T\text{: K}) \tag{3}$$

The solubility of CO_2 also depends on salinity. The effect of salinity on the solubility may be examined by considering the Setchenow equation[33] where α is the salting-out coefficient and $S‰$ is the salinity (assumed value is 34.321):

$$x_{CO_2} = \frac{f_{CO_2}}{H} e^{\alpha S‰} \tag{4}$$

The salting out coefficient is a function of temperature (in Kelvin) that is given by[34]

$$\alpha = 0.543 - 3.54 \times 10^{-3}T + 5.69 \times 10^{-6}T^2 \tag{5}$$

The surface tension of CO_2 (dyn/cm) is calculated as a function of T (°C) and critical temperature T_c (°C) from Quinn:[35]

$$\sigma_{CO_2} = 0.0653(T_C - T)^{1.24} \tag{6}$$

while for that of seawater (N/m, T in K, T_c = 647.15 K) is[36]

$$\sigma_W = 235.8 \times 10^{-3}\left(\frac{T_C - T}{T_c}\right)^{1.256}\left[1 - 0.625\left(\frac{T_C - T}{T_c}\right)\right] \tag{7}$$

The expression in eq 7 has been used also for gas particles.

Regarding clathrates (= hydrates), they are about instantaneously formed over liquid CO_2 droplets and more slowly on gas CO_2 or CH_4 bubbles. The precipitation of hydrates at the interface follows a very well (by now) understood mechanism, passing from nucleation to regular growing (description of which can be found, for instance, in refs 37–40). The time needed for the formation is very short compared to the time of CO_2 drops rising (or falling), and it has been considered acceptable and convenient to assume an instantaneous precipitation. The problem of hydrate layer, of course, is of extreme importance. As a matter of fact, the eventual presence of this rim has, essentially, an impact on the dissolution rate of the particles rising along the water column. Across the hydrate layer, the diffusion rate of the component finds an extra resistance that is reducing the resulting flux. However, following a reliable picture of the phenomena (well described by McGinnis et al.[25]), the sequence in the layer growing, when the particle moves, can be considered at the interface. The hydrate crystals do not form a compact layer, but they are independent one from the other. Due to the movement the hydrates, crystals are moving over the particle surface (of course toward the back side of the quasi-spherical particles). Consequently, along the rise, the distribution of the diffusional obstacle (i.e., the hydrate layer), along the particle surface, is not uniform. The sweeping activity of the fluid-dynamic shear has this consequence. Wherein the deposit is accumulated, the local flux of matter is reduced. When the kinetics of clathrates formation and dissolution are available, all these phenomena can be quantitatively described, but this information is not

available till now. The equation that characterizes the dissolution of the liquid or gas contained into the particle (drop or bubble) is the conventional mass balance:

$$\frac{dm_i}{dt} = -k_{C,i}\Delta C_i S_p MW_i \tag{8}$$

where $i = CO_2$ or CH_4; m_i = moles of component i; $k_{C,i}$ = mass transfer coefficient (for instance m/s) of component i; S_p = particle surface; MW_i = molecular weight of component i; t = time; ΔC_i = concentration difference between the equilibrium solubility of the gas and its aqueous concentration, defining the driving force for dissolution (for instance kmol/m^3).

Figure 1 shows a sketch of the concentration profile in the hydrate and the surrounding liquid: the hydrate thickness

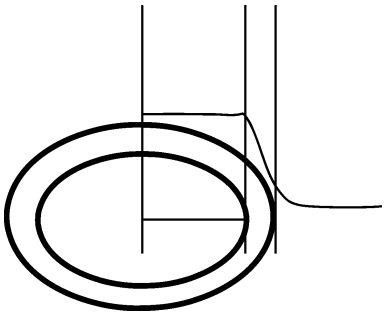

Figure 1. Sketch of the concentration profile in the hydrate and the surrounding liquid.

represented. The mass transfer resistance is related to the presence of the hydrate and to the boundary layer around the particle. I

We have simplified the problem by assuming that the contribution to the balance of the amount of gas dissolved in the clathrate layer and the breakage of bubbles (that is possible only for very large drops in the range 20−30 mm) can be neglected.

Of course, the time t depends on the distance traveled by the particle after the point of release and the evolution of its velocity:

$$t = \int \frac{dx}{V_p} \tag{9}$$

where x is the direction of movement and v_p is the particle rise velocity.

The mass transfer coefficient is of course the result of the superposition of all the resistances along diffusion path. By equating the fluxes (the radius of curvature is low so that the surface can be assumed as flat) the global mass transfer coefficient from particle surface (without hydrate)and surrounding water results as follows:

$$\frac{1}{k_T} = \frac{1}{k_H} + \frac{1}{k_F} \tag{10}$$

where k_T = total mass transfer coefficient; k_H = hydrate mass transfer coefficient; k_F = surrounding fluid mass transfer coefficient

The value of the hydrate layer contribution is evaluated from

$$k_H = \frac{D_{eff}}{\delta} \tag{11}$$

where δ is the hydrate thickness and D_{eff} is the diffusion coefficient inside the porous hydrates layer, depending on porosity ε and on tortuosity τ:

$$D_{eff} = \frac{\mathcal{D}\varepsilon}{\tau} \tag{12}$$

The value of $\mathcal{D}$ has been set to a value of 0.9×10^{-9} m^2/s.

The fluid mass transfer coefficient around the particle is a function also of the presence of the hydrate layer. As a matter of fact, the presence of hydrate, and, particularly, if the rim is covering the entire surface of the particle, inhibits the internal circulations. Consequently, the surrounding seawater in the relative motion resembles that one of a quasi-rigid particle. Then, the expression for the Sherwood number becomes that typical of the boundary layer theory:

$$Sh = 2 + 1.8(Re\cdot Sc)^{1/3} + 0.6Re^{1/2}Sc^{1/3} \tag{13}$$

with Reynolds number ($Re = (\rho_c D_0 v_P)/\mu_c$); μ_c = dynamic viscosity of the countinous phase; Schmidt number ($Sc = v_c/D$); $\mathcal{D}$ = diffusion coefficient of specie i inside the continuous phase; v_c = kinematic viscosity of the countinous phase; Sherwood number ($Sh = (k_c D_0)/D$). The proposed expression is a combination of contributes covering the variation of Re number during particle dissolution.

On the contrary, when the hydrate is absent, the interface is free to move. Because the viscosity of the fluid inside the particle is quite less than the viscosity of the seawater, the behavior for the Sherwood number becomes similar to the Higbie theory (see for instance in[41]), that is,

$$Sh = 2 + 1.12(Re\cdot Sc)^{1/2} \tag{14}$$

2.1. Rise Velocity. The calculation of the fluid dynamic velocity is necessary both for evaluating the fluid mass transfer coefficient and the time of particle rise after its release in the deep. In our model, the prevailing motion of the particle is assumed to be linear (secondary motions, i.e., helicoidal, zigzag, oscillating, etc., are neglected). Thanks to the mobility of the interface the fluid particle can modify its shape and can be characterized by internal circulations. The last ones strongly affects the resistance offered to the particle motion and the possible development of the boundary layer around the particle. The particle shape can be represented by the superposition of two semispheroids of different height and identical base areas (Figure 2).

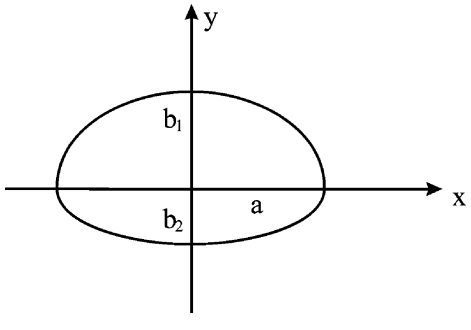

Figure 2. Assumed shape of the fluid particle (a, b_1, b_2 = particle major and minor semiaxes).

More specifically regarding the deformation, it is useful to mention that the hydrate deposits as a porous aggregate of microscopic particles and, therefore, is deformable together with the underlying particle.

In the steady state the forces balance (buoyant and friction forces) gives

$$\Delta\rho g V_p = \pi a^2 \frac{\rho_c V_p^2}{2} f \tag{15}$$

where V_p = particle volume; f = friction factor; a = particle major semiaxis. The terminal velocity (v_p) has been then deduced from eq 15 as a function of the drag coefficient C_D:

$$C_D = \left(\frac{2a}{D_0}\right)^2 f = \mathrm{Def}\cdot f \Rightarrow v_p = \left(\frac{4}{3}\frac{\Delta\rho g D_0}{\rho_c C_D}\right)^{1/2} \tag{16}$$

where Def = deformation factor.

The key variable in defining drop motion velocity becomes consequently the drag coefficient C_D that shows a simple dependence on the friction factor "f" and on the deformation. We have supposed that the particle assumes, during motion, a shape that minimizes its total energy. Substantially the energies mainly involved (interfacial, potential and kinetic, described in Bozzano and Dente[27]) reflect the influence of interfacial tension, density difference, viscosity and velocity on the particle shape. Contaminants or hydrates at the interface affect its rigidity and the internal circulations. The mapping of the total energy as a function of the particle geometrical properties allows, through its minimization, to deduce the deformation factor "Def". The shapes obtained by means of the minimization procedure have been correlated to the Morton ($\mathrm{Mo} = (\Delta\rho g\mu_c^4)/(\rho_c^2\sigma^3)$) and Eötvös numbers, giving an explicit expression for "Def" that avoids the minimization procedure during each calculation. The resulting deformation factor is then a function of the system physical properties and of the size of the particle:

$$\mathrm{Def} = \left(\frac{2a}{D_0}\right)^2 = \frac{10(1 + 1.3\mathrm{Mo}^{1/6}) + 3.1\mathrm{Eo}}{10(1 + 1.3\mathrm{Mo}^{1/6}) + \mathrm{Eo}} \tag{17}$$

The friction factor has been obtained by a combination of two asymptotic behaviors, viscous flow, f_{visc}, and Newton's-law flow, f_∞:

$$f(\mathrm{Re}, \mathrm{Eo}) = f_{visc}(\mathrm{Re}, \mathrm{Mo}) + f_\infty(\mathrm{Eo}, \mathrm{Mo}) \tag{18}$$

For spherical shape particles (Def = 1), and low Re values (about above 20 that is usually the case), the drag coefficient has been originally evaluated by Levich[42] and reviewed by Batchelor[43] by assuming that the rate at which buoyancy forces on the particle do work must be equal to the total rate of dissipation in the surrounding fluid:

$$C_D = f_{visc} = \frac{48}{\mathrm{Re}} \tag{19}$$

A correction was proposed by Moore,[44] taking into account also the dissipation in the boundary layer at the particle surface and in the wake

$$f_{visc} = \frac{48}{\mathrm{Re}}\left(1 - \frac{2.2}{\mathrm{Re}^{1/2}}\right) \tag{20}$$

Because in eq 20 the negative factor can give place to problems at low Re values, we propose a more satisfactory expression giving the same results but avoiding negative values:

$$f_{visc} = \frac{48}{\mathrm{Re}} \frac{\sqrt{1 + 0.25\mathrm{Re}}}{\sqrt{1 + 0.25\mathrm{Re}} + 1} \tag{21}$$

The motion can be also affected by the presence of circulations inside the fluid particle. No relative movement of the two fluids at the interface can occur and the tangential stress exerted at the interface by the external fluid must be equal and opposite to that exerted by the internal one.[43] The consequence is that the friction factor is affected by the viscosity ratio of the continuous and dispersed fluids, and this contribution can be accounted by a multiplying factor following the Hadamard−Rybczynski theory reported for instance in:[43]

$$f_{visc} = \frac{48}{\mathrm{Re}} \frac{\sqrt{1 + 0.25\mathrm{Re}}}{\sqrt{1 + 0.25\mathrm{Re}} + 1} \frac{3/2 + \mu_c/\mu_d}{1 + \mu_c/\mu_d} \tag{22}$$

Both the cases of drop ($\mu_c/\mu_d \ll 1$) and bubbles ($\mu_c/\mu_d \gg 1$) are covered by eq 22.

Finally, another contribution to eq 22 allows to take into account that in high viscosity medium; that is, for high Mo numbers, the factor "48" is reduced to "16". The resulting final expression of f_{visc} is

$$f_{visc} = \frac{48}{\mathrm{Re}} \frac{\sqrt{1 + 0.25\mathrm{Re}}}{\sqrt{1 + 0.25\mathrm{Re}} + 1} \frac{3/2 + \mu_c/\mu_d}{1 + \mu_c/\mu_d} \times \frac{1 + 12\mathrm{Mo}^{1/3}}{1 + 36\mathrm{Mo}^{1/3}} \tag{23}$$

The friction factor for sufficiently high Reynolds numbers (at least 10^4), becomes a constant (corresponding to a value of the drag coefficient of about 3) because of the large deformation (quasi-spherical cap shape). The asymptotic friction factor for high Reynolds numbers is also in this case deduced as function of Eo and Mo (by interpolation of the results obtained from the minimization procedure):

$$f_\infty = \frac{C_D|_\infty}{\mathrm{Def}|_\infty} = 0.9\frac{\mathrm{Eo}^{3/2}}{1.4(1 + 30\mathrm{Mo}^{1/6}) + \mathrm{Eo}^{3/2}} \tag{24}$$

The combined and final expression of the friction factor, covering all Re numbers, becomes (with c and d = indexes for continuous and dispersed phase):

$$f = \frac{48}{\mathrm{Re}} \frac{\sqrt{1 + 0.25\mathrm{Re}}}{\sqrt{1 + 0.25\mathrm{Re}} + 1} \frac{3/2 + \mu_c/\mu_d}{1 + \mu_c/\mu_d} \frac{1 + 12\mathrm{Mo}^{1/3}}{1 + 36\mathrm{Mo}^{1/3}} + 0.9\frac{\mathrm{Eo}^{3/2}}{1.4(1 + 30\mathrm{Mo}^{1/6}) + \mathrm{Eo}^{3/2}} \tag{25}$$

Internal circulations of drops are less intensive than inside bubbles, due to the higher viscosity, forcing the detachment of the boundary layer on a larger surface behind and retarding the transition to turbulence. Therefore, *for drop motion*, the friction factor is modified in

$$\text{For} \quad f_\infty < \beta \qquad f = \frac{48}{\mathrm{Re}} \frac{\sqrt{1 + 0.25\mathrm{Re}}}{\sqrt{1 + 0.25\mathrm{Re}} + 1} \frac{3/2 + \mu_c/\mu_d}{1 + +\mu_c/\mu_d} \frac{1 + 12\mathrm{Mo}^{1/3}}{1 + 36\mathrm{Mo}^{1/3}} + \beta$$

$$\text{For} \quad f_\infty < \beta \qquad f = \frac{48}{\mathrm{Re}} \frac{\sqrt{1 + 0.25\mathrm{Re}}}{\sqrt{1 + 0.25\mathrm{Re}} + 1} \frac{3/2 + \mu_c/\mu_d}{1 + +\mu_c/\mu_d} \frac{1 + 12\mathrm{Mo}^{1/3}}{1 + 36\mathrm{Mo}^{1/3}} + \alpha\frac{\mathrm{Eo}^{3/2}}{1.4(1 + 30\mathrm{Mo}^{1/6}) + \mathrm{Eo}^{3/2}} \tag{26}$$

The value of factor α has been set to 0.9, while that of β has been set to 0.45 for oblate spheroids (i.e., flattened at right

angles to the direction of motion) and to 0.3 for prolate spheroids (i.e., flattened in the direction of motion). This latter expression is valid also in the case of contaminated of hydrate covered bubbles. In fact, in this situation, bubbles have a drag coefficient close to that of a "rigid body", and therefore, internal circulations have no detectable influence on the dynamics of the bubble motion.

The assumed thickness (s_H) of the CO_2 hydrate has been 5.5 μm (in substantial agreement with the literature,[45] which reports an order of magnitude of about 7−8 μm). The suggested value for the CH_4 hydrate is about 15 μm in agreement with literature.[46] Regarding the rate of dissolution of hydrates (mol/s), the following expressions have been adopted making reference to the work of Clarke and Bihnoi:[47]

$$N_H = K\cdot\exp\left(-\frac{E_H}{RT}\right)RT(C_i - C_b)S_H \tag{27}$$

where K = kinetic constant for the hydrate dissolution = 3.6×10^4 (mol/s·Pa·m^2) for CH_4 and 1.83×10^8 (mol/s·Pa·m^2) for CO_2; S_H = hydrate surface = hydrate specific surface SSH = 3.75×10^5 (m^2/m^3) multiplied by the hydrate volume; E_H = activation energy for hydrate formation and dissolution (81 kJ/mol for CH_4 and 102.88 kJ/mol for CO_2); R = gas constant 8.31447 (J/K·mol); C_i = concentration of the guest specie at the particle interface; C_b = concentration of the guest specie in the bulk of the surrounding phase (78 ppm for CO_2 and 0 ppm for CH_4).

The hydrate volume has been evaluated as follows:

$$V_H = \frac{4}{3}\pi\left[\left(\frac{D_p + 2S_H}{2}\right)^3 - \left(\frac{D_p}{2}\right)^3\right] \tag{28}$$

The hydrate density (ρ_H) can be evaluated by using the expression of Teng et al.[48] that is consistent with experimental data:

$$\rho_H = \frac{46MW_i}{a^3}N\left(0.409 + \frac{X_{iH}}{1 - X_{iH}}\right) \tag{29}$$

where N = Avogadro number = 6.022×10^{23}; x_{iH} = mole fraction of guest specie "i" inside the hydrate; a = reticulation constant (m) = 12×10^{-10}; MW_i = molecular weight of the guest specie.

RESULTS AND DISCUSSION

In this paper, only few representative examples of the many results obtained by means of the presented model are shown. In the following figures, the points represent the experimental data taken from the literature.[20,25,49] The lines refer to the model predictions. Let us start with the data from Brewer et al.[20] that we have resumed in Table 1. An equipment able to follow the drops during they rise from deep ocean called "ROV Ventana" was used. The data refer to an experiment performed by releasing a first CO_2 drop (a) at a depth of 804.5 m. At about 650 m this droplet was joined by a second drop (b). Then, quickly the pair of drops joined, without coalescing (because of the protective clathrate layer). The cohesive force maintained the pair together till the dissolution of the first one. When the remaining of the second drop reached a depth of about 400 m, liquid−gas transition started. The quasi-linear evolution of vaporization dictates the progressive decrease of the mixed phase density (hypothetically the final part of this phenomenon takes end when the "virtual" depth reaches about 100−150 m).

Table 1. Experimental Data from Brewer et al.[25]

elapsed time (min)	depth (m)	temp. (°C)	droplet diam. (cm) (a)	droplet diam. (cm) (b)	CO_2 density (g/cm^3)	rise rate (cm/s)
0	804.3	4.39	0.890		0.942	10.2
14.23	706.3	4.74	0.606		0.931	11.3
23.13	649.1	4.99	0.485	0.890	0.923	12.0
29.82	602.1	5.26	0.364	0.728	0.917	12.5
43.08	496.8	5.44	0.162	0.647	0.902	13.5
49.73	447.3	5.99		0.364	0.891	14
61.65	341.2	7.29		0.202	0.863	14.9

Table 2. Experimental and Calculated Drop Velocity

depth (m)	exptl. rise rate (cm/s)	calcd. rise rate (cm/s)
804.3	10.2	11.7
706.3	11.3	11.4
649.1	12.0	12.5
602.1	12.5	12.3
496.8	13.5	12.0
447.3	14	11.0
341.2	14.9	12.8

Figures 3 and 4 show the comparison with the results of our model. In both, the diameter evolution along the time (a) and along the depth (b) is compared.

It is important to observe that both the dependence of bubble diameter on time and depth is well simulated. It means that the bubble rise velocity is properly evaluated. Figure 5 shows the comparison between the calculated and experimental liquid CO_2 density. Also, in this case, the comparison is satisfactory.

The simulations performed for the second drop (b) released at 649.1 requested to take into account that at about 400 m depth the liquid CO_2 starts to evaporate. This affects the density of the droplet and, consequently, its rise velocity, so that an acceleration has been detected. Table 2 reports also the comparison with the droplet rise velocity.

The comparison of Table 2 is satisfactory except for the three last point. From 649.1 to 496.8 m depth the two droplet moves together and the velocity has been evaluated taking into account a diameter equivalent to the volume obtained from the sum of the volume of the two droplets. At the depth of 447.3 the first drop released is about completely consumed. Moreover, no evaporation is present, so we are not able to find a reason for the rise rate found in the experiments that cannot be related simply to the reduction of drop density. At 341.2 m depth vaporization is present (it starts at about 409 m depth): the fluid particle becomes constituted in part by liquid and partially vaporized. We assumed an average density taking into account the degree of vaporization (massive fraction of vapor) evaluated as the ratio between the difference of actual pressure and that of initial vaporization (Pvap1) and the difference between the pressure at 100 m (where vaporization is complete) and Pvap1. Pressures are in Pa.

$$\text{vapgrade} = \frac{P - P_{vap1}}{10^6 - P_{vap1}} \tag{30}$$

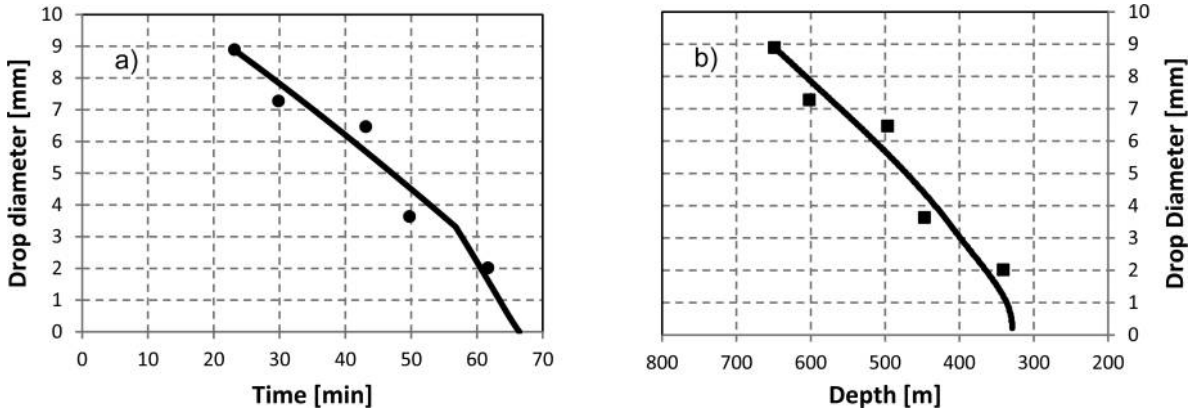

Figure 3. Drop diameter as a function of (a) time (drop starting at 649.1 m depth) and (b) depth (drop starting at 649.1 m depth).

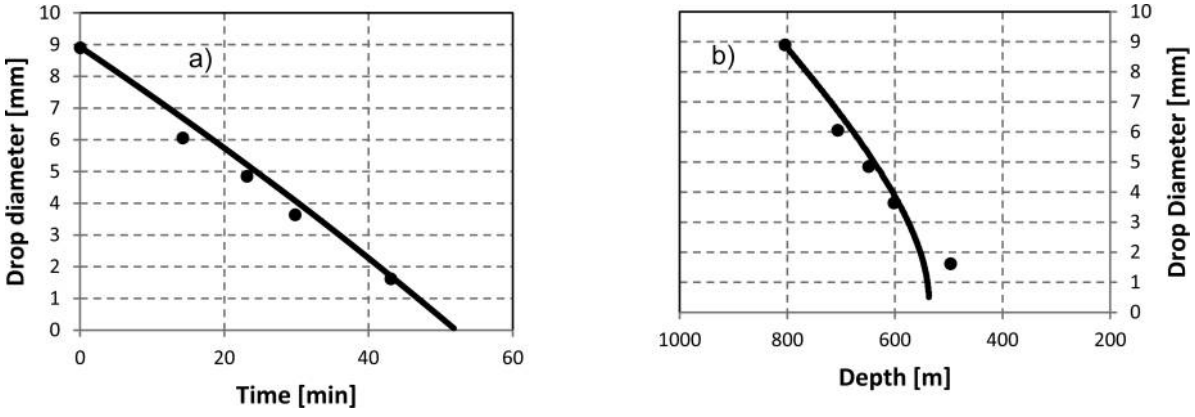

Figure 4. Drop diameter as a function of (a) time (drop starting at 805.4 m depth) and (b) depth (drop starting at 805.4 m depth).

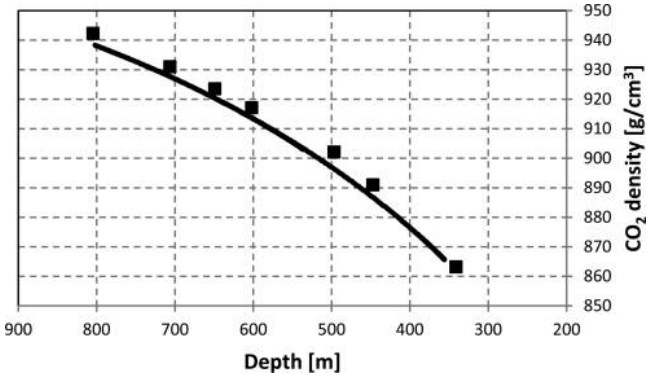

Figure 5. Experimental and calculated CO_2 density.

We have deduced then the mass of liquid and vapor and obtain the value of rise velocity by a simple combination of the velocity calculated considering the particle all liquid and all vaporized.

$$v = \frac{v_d m_L + v_b m_v}{m_L + m_v} \tag{31}$$

In eq 31, V_d is the velocity of the particle considered liquid, v_b is the velocity of the particle considered completely vaporized, m_L and m_v respectively the liquid and vapor mass contained into the particle.

A comparison of the rate of dissolution of CH_4 bubbles is then reported. The data are taken from the paper of McGinnis et al.,[25] which elaborated the data of Rehder et al.[50]

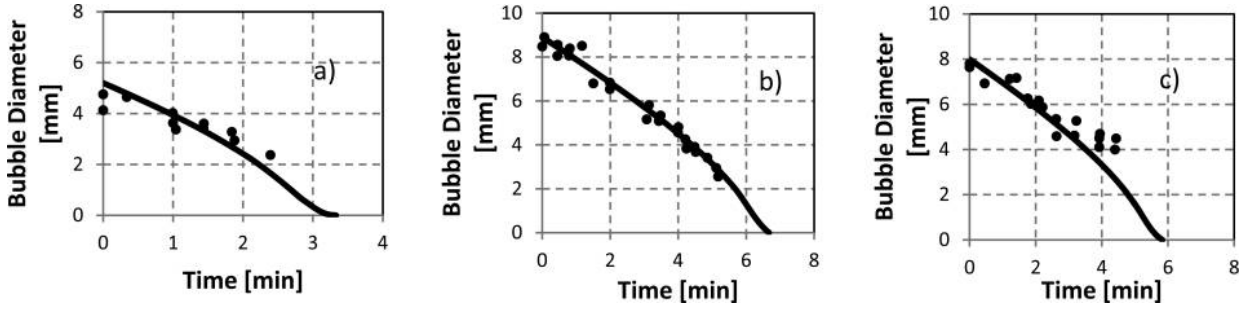

Figure 6. Dissolution of CH_4 bubbles.

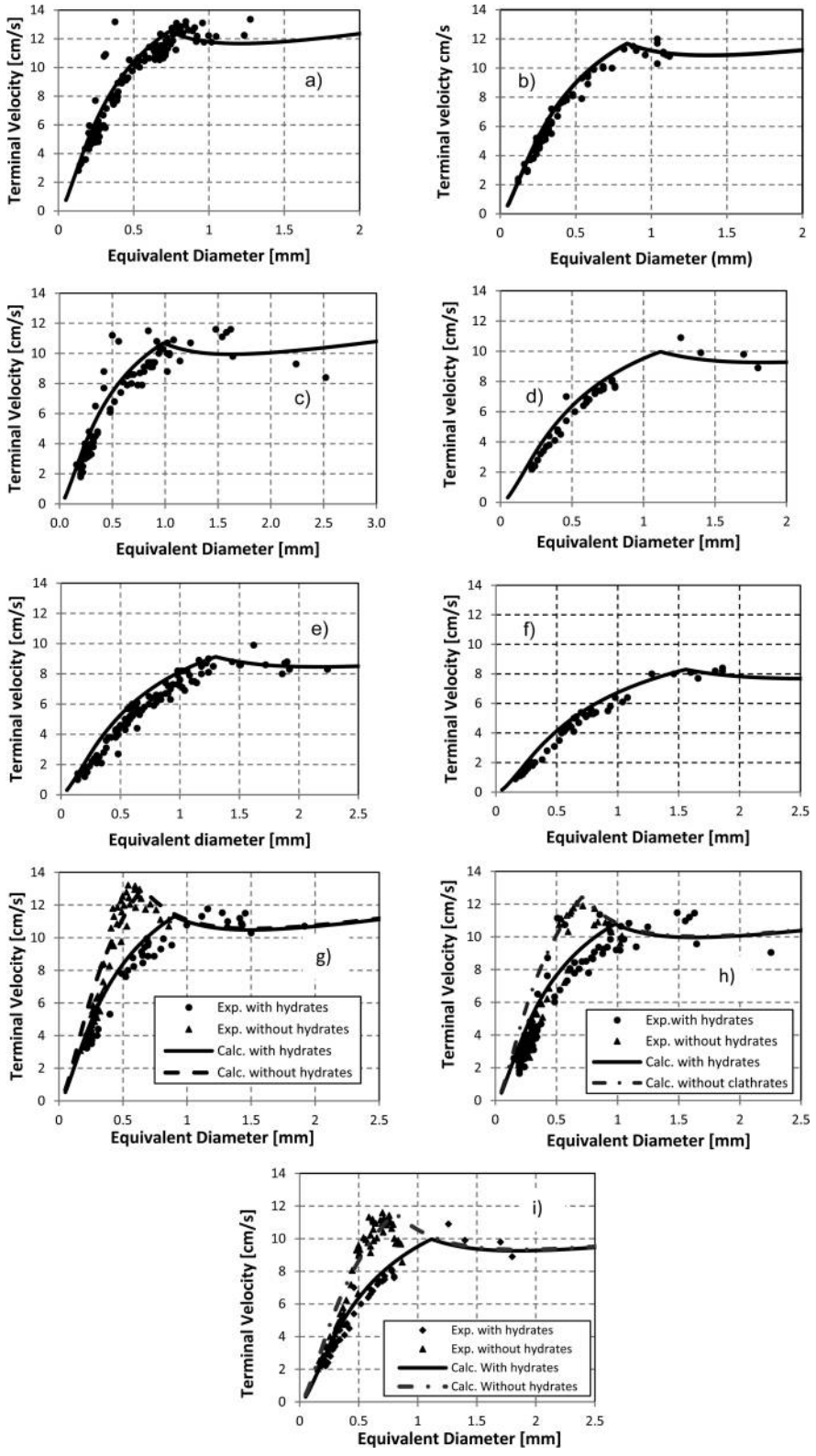

Figure 7. Drop terminal velocity versus equivalent diameter. (a–f) Experiments in hydrate formation conditions. (a) 5.7 MPa, T = 4.8 °C, (b) P = 8.3 MPa – T = 3.6 °C, (c) 11.9 MPa, 2.8 °C, (d) 14.7 MPa, 2.5 °C, (e) P = 17.5 MPa – T = 2 °C, (f) 20.2 MPa, 1.9 °C. (g–i) comparison between hydrate and no-hydrate conditions: (g) hydrate formation conditions (9.9 MPa, 3.2 °C) and no hydrate (18.3 MPa, 13.1 °C), (h) hydrate formation conditions (11.9 MPa, 2.8 °C) and no hydrate (22 MPa, 13.9 °C), (i) hydrate formation conditions (14.7 MPa, 2.5 °C) and no hydrate (24.8 MPa, 13.1 °C).

The experiments refer to the release of methane bubbles of varying diameter at different depths. Measurements were made using the same equipment already mentioned for CO_2, the ROV Ventana, in Monterey Bay, California. Here the upper boundary of the methane hydrate stability field is close to 520 m depth.[51] Single gas bubbles were released at various

Table 3. Experimental Data from Bigalke et al.[49]

pressure (Mpa)	temp. (°C)	CO_2 density (g/cm^3)	sea water density (g/cm^3)	hydrate stable	calcd. interfacial tension (dyn/cm)
5.7	4.8	915.1	1030.3	yes	34.2
8.3	3.6	943.9	1031.7	yes	33.9
9.9	3.2	957.0	1032.4	yes	33.7
11.9	2.8	971.1	1033.4	yes	33.6
14.7	2.5	987.2	1034.7	yes	33.2
17.5	2.0	1002.4	1036.1	yes	32.7
20.2	1.9	1014.1	1037.3	yes	32.3
18.3	13.1	958.7	1034.2	no	35.0
22.0	13.9	973.9	1036.3	no	34.8
24.8	13.1	989.5	1037.0	no	34.3

depths between 820 and 430 m into an imaging box attached to the ROV. Figure 6a refers to the release of a bubble of methane of 5.2 mm initial diameter. The start depth is 426 m. The experimental end depth is 386 m, while in our simulations a value of 379 m has been obtained. Figure 6b refers to the release of a bubble of methane of 8.9 mm initial diameter. The start depth is 471 m. The experimental end depth is 394 m, while in our simulations a value of 374 m has been obtained. Figure 6c refers to the release of a bubble of methane of 8 mm initial diameter. The start depth is 479 m. The experimental end depth is 433 m, while in our simulations a value of 395 m has been obtained. Figure 6 shows that the dissolution as a function of time is well represented by the model also in the case of CH_4 bubbles.

A further comparison of the rise velocity of CO_2 droplets has been performed with the experiment of Bigalke et al.[48] and is reported in Figure 7. The operating conditions selected by Bigalke et al. cover a large range and they performed experiments in P/T conditions both within and outside the hydrate stability field simulating in a laboratory tank an oceanic temperature depth profile. The data related to the experiments of Bigalke et al. are reported in Table 3.

The last column of Table 3 reports the interfacial tension calculated by using the equation of our model. We have adopted the same kind of representation as in the paper of Bigalke et al.[28] The general agreement with experimental data is satisfactory. It can be observed that in some cases (for instance, Figure 7a and c) the experimental points show for the same equivalent diameter isolated points at higher rise velocity. This could be related to an assumed shape of the drop similar to a prolate spheroid allowing a lesser drag coefficient during motion.

Parts g, h, and i of Figure 7 report data related to the rise velocity of CO_2 droplet covered by hydrates (lower data points) and of CO_2 droplets outside the hydrate formation conditions. In this latter case, in order to simulate the droplets behavior we have used the value of parameter β equal to 0.3 in eq 26, while in the case of droplets covered with clathrates the assumed value is 0.45. This is due to the assumption, deduced from the droplets aspect ratio reported by Bigalke et al.,[49] that the shape of the droplet is that of a oblate spheroid in the case of presence of the hydrate, while when the latter is absent the shape assumed by the droplet is that of a prolate spheroids. It justifies also the higher the rise velocities.

Figure 8 shows a sensitivity study of parameters α and β of eq 26.

It can be observed that the variation of parameter α generated a shift of the maximum maintaining the same initial slope of the simulated curve while varying β the initial slope is changing.

CONCLUSIONS

In this paper, a model describing the rise rate and the progressive dissolution of CO_2 and CH_4 drop and bubbles eventually emerging from the deep ocean has been presented. For both the aspects that have been examined (fluid-dynamics and mass transfer in extreme conditions) and for both the components, the comparison of the simulations with experimental data is satisfactory. It is important to point out that the fluid-dynamic model here presented is not the results of the fitting of experimental data but it is general for all gas−liquid and liquid−liquid systems. It can be observed that for the drop sizes analyzed the rate of consumption is such that the particle does not reach the sea surface and is dissolved during its motion.

AUTHOR INFORMATION

Corresponding Author

*E-mail: giulia.bozzano@polimi.it. Phone: +39 (0)2 2399 3094. Fax: +39 (0)2 7063 8173.

Notes

The authors declare no competing financial interest.

ACKNOWLEDGMENTS

Authors acknowledge Gianvito Vilè for his collaboration and for the discussions during the initial development of the model.

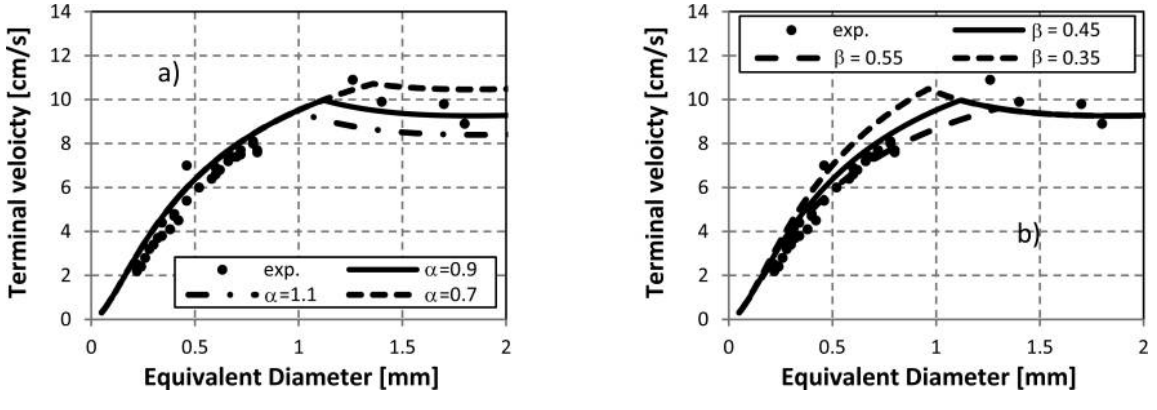

Figure 8. Sensitivity study of parameters (a) α and (b) β.

REFERENCES

(1) Kvenvolden, K. A. Methane Hydrate—A Major Reservoir of Carbon in the Shallow Geosphere. *Chem. Geol.* **1988**, *71*, 41.

(2) MacDonald, G. J. The Future of Methane as an Energy Resource. *Annu. Rev. Energy* **1990**, *15*, 53.

(3) Gornitz, V.; Fung, I. Potential Distribution of Methane Hydrate in the World's Oceans. *Glob. Biogeochem. Cycles* **1994**, *8*, 335.

(4) Lelieveld, J.; Crutzen, P. J. Changing Concentration, Lifetime and Climate Forcing of Atmospheric Methane. *Tellus* **1998**, *50 B*, 1284.

(5) Katz, M. E.; Pak, D. K.; Dickens, G. R.; Miller, K. G. The Source and Fate of Massive Carbon Input During the Latest Paleocene Thermal Maximum. *Science* **1999**, *286*, 1531.

(6) *Special Report on Carbon Dioxide Capture and Storage: Intergovernmental Panel on Climate Change*; Cambridge University Press: Cambridge, 2005; available at http://www.ipcc-wg3.de/special-reports/special-report-on-carbon-dioxide-capture-and-storage.

(7) Park, Y.; Kim, D. Y.; Lee, J. W.; Huh, D. G.; Park, K. P.; Lee, J.; Lee, H. Sequestering Carbon Dioxide into Complex Structures of Naturally Occurring Gas Hydrates. *Proc. Natl. Acad. Sci. U.S.A.* **2006**, *103* (34), 12690.

(8) Hofmann, M.; Schellnhuber, H. S. Ocean Acidification: A Millennial Challenge. *Energy Environ. Sci.* **2010**, *3*, 1883.

(9) Sloan, E. D.; Koh, C. A. *Clathrate Hydrates of Natural Gases*, 3rd ed.; CRC Press: New York, 2008.

(10) International Maritime Organization. Carbon Capture and Sequestration, 2006;http://www.imo.org/OurWork/Environment/LCLP/EmergingIssues/CCS/Pages/default.aspx (accessed Jan 2014).

(11) Sakai, H.; Gamo, T.; Kim, E. S.; Tsutsumi, M.; Tanaka, T.; Ishibashi, J.; Wakita, H.; Yamano, M.; Oomori, T. Venting of Carbon Dioxide-Rich Fluid and Hydrate Formation in Mid-Okinawa Trough Backarc Basin. *Science* **1990**, *248*, 1093.

(12) Lupton, J.; Butterfield, D.; Lilley, M.; Evans, L.; Nakamura, K.; Chadwick, W., Jr.; Resing, J.; Embley, R.; Olson, E.; Proskuriwski, G.; Baker, E.; de Ronde, C.; Roe, C.; Greene, R.; Lebon, G.; Young, C. Submarine Venting of Liquid Carbon Dioxide on a Mariana Arc Volcano. *Geochem. Geophys. Geosyst.* **2006**, *7*, Q08007.

(13) Radhakrishnan, R.; Demurov, A.; Herzog, H.; Trout, B. L. A Consistent and Verifiable Macroscopic Model for the Dissolution of Liquid CO_2 in Water under Hydrate Forming Conditions. *Energy Convers. Manage.* **2003**, *44*, 771.

(14) Hirai, S.; Okazaki, K.; Tabe, Y.; Hijikata, K.; Mori, Y. Dissolution Rate of Liquid CO_2 in Pressurized Water Flows and the Effect of Clathrate Films. *Energy* **1997**, *22*, 285.

(15) Hirai, S.; Okazaki, K.; Araki, N.; Yazawa, H.; Ito, H.; Hijikata, K. Transport Phenomena of Liquid CO_2 in Pressurized Water Flow with Clathrate Hydrate at the Interface. *Energy Convers. Manag.* **1996**, *37*, 1073.

(16) Haljasmaa, I. V.; Vipperman, J. S.; Rea, D. K.; Owen, R. M. Control of a Fluid Particle Under Simulated Deep-Ocean Conditions in a High-Pressure Water Tunnel. *Rev. Sci. Instrum.* **2005**, *76*, 025111.

(17) Ozaki, M.; Minamiura, J.; Kitajima, Y.; Mizokami, S.; Takeuchi, K.; Hatakenaka, K. CO_2 Ocean Sequestration by Moving Ships. *J. Mar. Sci. Technol.* **2001**, *6*, 51 ex 18.

(18) Maini, B. M.; Bishnoi, P. R. Experimental Investigation of Hydrate Formation Behavior of a Natural Gas Bubble in a Simulated Deep Sea Environment. *Chem. Eng. Sci.* **1981**, *36*, 183.

(19) Rehder, G.; Kirby, S. H.; Durham, W. B.; Stern, L. A.; Peltzer, E. T.; Pinkston, J.; Brewer, P. Dissolution Rates of Pure Methane Hydrate and Carbon Dioxide Hydrate in Undersaturated Seawater at 1000-m Depth. *Geochim. Cosmochim. Acta* **2004**, *68*, 285 ex 19.

(20) Brewer, P. G.; Peltzer, E. T.; Friederich, G.; Rehder, G. Experimental Determination of the Fate of Rising CO_2 Droplets in Seawater. *Environ. Sci. Technol.* **2002**, *36*, 5441.

(21) Tsouris, C.; Brewer, P. G.; Peltzer, E. T.; Walz, P.; Riestenberg, D.; Liang, L.; West, O. R. Hydrate Composite Particles for Ocean Carbon Sequestration: Field Verification. *Environ. Sci. Technol.* **2004**, *38*, 2470.

(22) Chen, B.; Song, Y.; Nishio, M.; Akai, M. Large Eddy Simulation of Double Plume Formation Induced by CO_2 Dissolution in the Ocean. *Tellus* **2003**, *55B*, 723.

(23) Zhang, Y. Fate of Rising CO_2 Droplets in Seawater. *Environ. Sci. Technol.* **2005**, *39*, 7719.

(24) Gangstø, R.; Haugan, P. M.; Alendal, G. Parameterization of Drag and Dissolution of Rising CO_2 Drops in Seawater. *Geophys. Res. Lett.* **2005**, *32*, L10612.

(25) McGinnis, D. F.; Greinert, J.; Artemov, Y.; Beaubien, S. E.; Wüest, A. Fate of Rising Methane Bubbles in Stratified Waters: How Much Methane Reaches the Atmosphere? *J. Geophys. Res.: Oceans (1978–2012)* **2006**, *111*, C09007 ex. 26.

(26) Rehder, G.; Leifer, I.; Brewer, P. G.; Peltzer, E. T. Controls on Methane Bubble Dissolution Inside and Outside the Hydrate Stability Field from Open Ocean and Atmosphere. *Geo-Mar. Lett.* **2009**, *22*, 198.

(27) Bozzano, G.; Dente, M. Shape and Terminal Velocity of Single Bubble Motion: A Novel Approach. *Comput. Chem. Eng.* **2001**, *25*, 571.

(28) Bigalke, N. K.; Enstad, L. I.; Rehder, G.; Alendal, G. Terminal Velocities of Pure and Hydrate Coated CO_2 Droplets and CH_4 Bubbles Rising in a Simulated Oceanic Environment. *Deep Sea Research Part I: Oceanographic Research Papers* **2010**, *57*, 1102.

(29) Bozzano, G.; Dente, M. Single Bubble and Drop Motion Modeling. *Chem. Eng. Trans.* **2009**, *17*, 567.

(30) Peng, D. Y.; Robinson, D. B. A New Two-Constant Equation of State. *Ind. Eng. Chem. Fundam.* **1976**, *15* (1), 59.

(31) Patel, N. C.; Teja, A. S. A New Equation of State for Fluids and Fluid Mixtures. *Chem. Eng. Sci.* **1982**, *37* (3), 463.

(32) Reid, R. C.; Prausnitz, J. M.; Poling, B. E. *The Properties of Gases and Liquids*; McGraw-Hill International: Singapore, 1988.

(33) King, M. B. *Phase Equilibrium in Mixtures*; Pergamon Press: London, 1969.

(34) Teng, H.; Yamasaki, A. Solubility of Liquid CO_2 in Synthetic Sea Water at Temperatures from 278 to 293 K and Pressures from 6.44 to 29.49 MPa, and Densities of the Corresponding Aqueous Solutions. *J. Chem. Eng. Data* **1998**, *43*, 2.

(35) Quinn, E. L. The Surface Tension of Liquid Carbon Dioxide. *J. Am. Chem. Soc.* **1927**, *49* (11), 2704.

(36) Vargaftik, N. B.; Volkov, B. N.; Voljak, L. D. International Tables of the Surface Tension of Water. *J. Phys. Chem. Ref. Data* **1983**, *12*, 817.

(37) Heeschen, K.; Keir, R. S.; Rehder, G.; Klatt, O.; Suess, E. Methane Dynamics in the Weddell Sea Determined via Stable Isotope Ratios and CFC-11. *Glob. Biogeochem. Cycles* **2004**, 18.

(38) Hester, K. C.; Peltzer, E. T.; Dunk, R. M.; Walz, P.; Brewer, P. G. Can Hydrate Dissolution Experiments Predict the Fate of a Natural Hydrate System? *Proceedings of the 6th International Conference on Gas Hydrates (ICGH 2008)*, Vancouver, British Columbia, Canada, July 6–10, 2008

(39) Kishimoto, M.; Iijima, S.; Ohmura, R. Crystal Growth of Clathrate Hydrate at the Interface between Seawater and Hydrophobic-Guest Liquid: Effect of Elevated Salt Concentration. *Ind. Eng. Chem. Res.* **2012**, *51*, 5224.

(40) Tanaka, R.; Sakemoto, R.; Ohmura, R. Crystal Growth of Clathrate Hydrates Formed at the Interface of Liquid Water and Gaseous Methane, Ethane, or Propane: Variations in Crystal Morphology. *Cryst. Growth Des.* **2009**, *9*, 2529.

(41) Bird, R. B.; Stewart, W. E.; Lightfoot, E. N. Transport Phenomena: Wiley: New York, 1960.

(42) Levich, V. G. *Physico-chemical Hydrodynamics*; Prentice-Hall: New York, 1962.

(43) Batchelor, G. K. *An Introduction to Fluid Dynamics*: Cambridge University Press: Cambridge, 1970.

(44) Moore, D. W. The Boundary Layer on a Spherical Gas Bubble. *J. Fluid Mech.* **1963**, *16*, 161.

(45) Abe, Y.; Abe, Y.; Aya, I.; Yamane, K. The Optical Measurement of CO_2 Clathrate Hydrate Membrane Thickness. *J. Therm. Sci. Technol.* **2006**, *2* (1), 13.

(46) Li, S.; Sun, C.; Liu, B.; Feng, X.; Li, F.; Chen, L.; Chen, G. Initial Thickness Measurements and Insights into Crystal Growth of Methane Hydrate Film. *AIChE J.* **2013**, *59*, 2145.
(47) Clarke, A. M.; Bishnoi, P. R. Determination of the Intrinsic Rate Constant and Activation Energy of CO_2 Gas Hydrate Decomposition Using In-situ Particle Size Analysis. *Chem. Eng. Sci.* **2004**, *59*, 2983.
(48) Teng, H.; Yamasaki, A.; Shindo, Y. Stability of the Hydrate Layer Formed on the Surface of a CO_2 Droplet in High-Pressure, Low-Temperature Water. *Chem. Eng. Sci.* **1996**, *51*, 4979.
(49) Bigalke, N. K.; Rehder, G.; Gust, G. Experimental Investigation of the Rising Behavior of CO_2 Droplets in Seawater Under Hydrate Forming Conditions. *Environ. Sci. Technol.* **2008**, *42*, 5241.
(50) Rehder, G.; Brewer, P. W.; Peltzer, E. T.; Friederich, G. Enhanced Lifetime of Methane Bubble Streams Within the Deep Ocean. *Geophys. Res. Lett.* **2002**, *29*, 15−17, 31.
(51) Peltzer, E. T.; Brewer, P. G. *Natural Gas Hydrate in Oceanic and Permafrost Environments*; Academic Publishers: Dordrecht, The Netherlands, 2000.